Oceanologia (2020) 62, 126—138

Available online at www.sciencedirect.com

ScienceDirect

journal homepage: www.journals.elsevier.com/oceanologia

ORIGINAL RESEARCH ARTICLE

Indian Ocean wind speed variability and global teleconnection patterns

Mourani Sinha[a,*], **Somnath Jha**[b], **Paromita Chakraborty**[c]

[a] *Department of Mathematics, Techno India University, Saltlake, Kolkata, India*
[b] *Department of Home, Swami Vivekananda State Police Academy, Barrackpore, India*
[c] *National Centre for Medium Range Weather Forecasting, Noida, Uttar Pradesh, India*

Received 23 February 2019; accepted 11 October 2019
Available online 30 October 2019

KEYWORDS
Wind speed;
Sea surface temperature;
Monsoon;
Wavelet coherence;
Indian Ocean;
Global teleconnection

Summary The influence of the local sea surface temperature (SST) and remote ENSO (El Niño-Southern Oscillation) indices on the wind speed (WS) data were explored for the Indian Ocean region. Relationships among the parameters were studied using spatial correlation plots and significant correlation ranges. Two months (July and January) representing opposite monsoon phases were selected for analysis for the period 1950—2016. There was a significant negative correlation between WS and SST over the Bay of Bengal (BOB) during July. Although different ENSO indices correlated differently in different areas of the Indian Ocean, the region off the coast of Sri Lanka was most significantly teleconnected. The southwest monsoon locally impacted the WS and SST relationship and the WS parameter was remotely teleconnected in both the monsoon seasons. Further empirical orthogonal function (EOF) analysis was applied on the 67 years WS data of the BOB region to extract the dominant mode representing maximum variability of the total variance. The temporal pattern of the first principal component (PC1) of WS data was linked to the North Atlantic Oscillations in January and the Atlantic Multidecadal Oscillation in July respectively. The continuous wavelet power spectra of the PC1 of WS showed significant regions in the 2—4-year band resembling the ENSO variability. Wavelet coherence applied between PC1 of WS and the ENSO indices showed greatest values for January in the 8—16-year band and for July in the 0—4-year band. A close relationship was established between the WS variability in BOB and the ENSO indices.
© 2020 Institute of Oceanology of the Polish Academy of Sciences. Production and hosting by Elsevier B.V. This is an open access article under the CC BY-NC-ND license (http://creativecommons.org/licenses/by-nc-nd/4.0/).

* Corresponding author at: Department of Mathematics, Techno India University, Saltlake, Kolkata 700091, India. Tel.: +91 9350904194
E-mail address: mou510@gmail.com (M. Sinha).
Peer review under the responsibility of the Institute of Oceanology of the Polish Academy of Sciences.

Production and hosting by Elsevier

https://doi.org/10.1016/j.oceano.2019.10.002
0078-3234/© 2020 Institute of Oceanology of the Polish Academy of Sciences. Production and hosting by Elsevier B.V. This is an open access article under the CC BY-NC-ND license (http://creativecommons.org/licenses/by-nc-nd/4.0/).

1. Introduction

Several studies reveal the impact of the Indian Ocean in shaping the climate on both regional and, global scales (Dong and McPhaden, 2018; Kug and Kang, 2006; Okomura and Deser, 2010). There are modes of climate variability, ranging from intraseasonal to interannual and, also longer time scales. The ENSO is the most significant interannual mode of tropical coupled ocean-atmosphere phenomenon (McPhaden, 2002). The inverse relationship between Indian summer monsoon rainfall and, ENSO (Kumar et al., 1999) was modulated on decadal timescales and, its changes were linked to Atlantic Multidecadal Oscillation (Chen et al., 2010), aerosol impacts (Azad and Rajeevan, 2016) and, zonal shifts in ENSO's center from eastern Pacific to central Pacific (Fan et al., 2017). The summer variability over the Indo-Northwest Pacific region was studied (Xie et al., 2016) in reference to the occurrence of a large-scale anomalous anticyclone in post-El Niño summers over the tropical Northwest Pacific and North Indian oceans. Li et al. (2017) discussed various theories relating to the formation, development, and maintenance of the western North Pacific anomalous anticyclone that transfers El Niño's impact on East Asian climate. Sun and Wang, (2019) revealed a connection between the summer climate of the Three-River-Source region of China and the global climate system in terms of North Atlantic Oscillation, western Indian Ocean sea surface temperature, El Niño-Southern Oscillation, and the East Asian summer monsoon. During an El Niño event, there were positive SST anomalies over the Indian Ocean from 3 to 6 months after SST anomalies peak in the tropical Pacific (Klein et al., 1999). The interannual Indian Ocean SST variations were positively correlated with the eastern equatorial Pacific Ocean SST anomalies with a lag of about 4 months (Venzke et al., 2000). Li et al. (2001) analyzed that although the eastern Pacific SST affects the monsoon on the ENSO time scale (2—7 year), the Indian monsoon rainfall had significant positive correlations with the Indian Ocean SST on the tropical biennial oscillation time scale (2—3 year). The warming in the Indian Ocean produced an easterly wind stress anomaly over Indonesia and, the western Pacific during the mature phase of El Niño (Kug and Kang, 2006). The easterly wind stress anomaly over the western Pacific, as mentioned above, lead to the rapid termination of El Niño and a fast transition to La Niña by generating upwelling Kelvin waves. The Indian Ocean warming which was effective for relatively strong El Niños resulted in La Niña one year after the mature phase of El Niño (Kug and Kang, 2006). A review was performed based on the climatic importance of Indian Ocean SST and the role of ocean dynamics in their generation (Schott et al., 2009). A possible role of the Indian Ocean was identified in the asymmetric evolution of surface wind anomalies over the western Pacific (Okomura and Deser, 2010). The relationship between sea surface temperature anomaly (SSTA) and, wind energy input in the Pacific Ocean was studied from 1949 to 2003 (Huang and Qiao, 2009). They showed a strong negative correlation between SSTA and, local wind energy input to surface waves in most of the domains at low and middle latitudes. Huang and Qiao (2009) also indicated wind energy input may play an important role in the interannual and decadal variability of the wind parameter in the Pacific Ocean by regulating vertical mixing processes in the upper ocean. The varied wind energy input over the past decades may lead to varied mixing in the upper ocean which may affect the SST and, then the global climate system. The role of the Indian Ocean was observed in initiating El Niño events, their development and fading away (Annamalai et al., 2005). Dong and McPhaden (2018) suggested warm SSTs in the Indian Ocean in 2014 weakened westerly wind anomalies in the Pacific which suppressed the development of the El Niño in 2014. Goswami et al. (2006) identified warm (cold) phases of the Atlantic Multidecadal Oscillation (AMO) producing increased (decreased) Indian summer monsoon rainfall and negative (positive) North Atlantic Oscillation (NAO) events resulting in below (above) normal monsoon rainfall. Through the NAO they established a fundamental link between the North Atlantic and the Indian summer monsoon. Thus the Indian Ocean is connected with the different climatic oscillations around the world.

In this study, the variability of the wind speed parameter in the BOB region was explored for possible teleconnection patterns across the globe. Several statistical tools like empirical orthogonal function analysis, wavelet analysis, wavelet coherence, significant correlation ranges have been used and are discussed in methodology. The wind speed is a major parameter for monitoring and predicting extreme weather patterns. It affects the development of surface waves and storm surges. In this paper, the impact of local SST and remote ENSO indices on the wind speed parameter in the Indian Ocean region was discussed. A connection was explored linking the relationship between WS variability and the ENSO indices in the BOB region.

2. Data and methodology

NCEP/NCAR reanalysis monthly mean surface (0.995 sigma level) WS data were available at 2.5-degree latitude by 2.5-degree longitude global grid. WS data were extracted for July and January for the Indian Ocean region covering the area from 30°E to 120°E and 30°N—70°S for the period 1950—2016. NOAA Extended Reconstructed Sea Surface Temperature V4 data were available at 2.0-degree latitude by a 2.0-degree longitude global grid. SST data were extracted for the above region for the same period. WS and SST data were interpolated to 1.0-degree by 1.0-degree spatial resolution for uniformity in dimension required during the statistical analysis.

For the present work the month of July, representing the southwest monsoon and the month of January, representing the northeast monsoon, have been analyzed for particular years of the period 1950—2016 and classified as normal or El Niño or La Niña months following the Oceanic Nino Index (ONI) standard. The ONI is a three month average of SST anomalies in the Niño 3.4 region (5°N—5°S, 120°—170°W), based on 30-year base periods updated every 5 years. The extended reconstructed sea surface temperature, version 5 (ERSSTv5) has been updated and improved (Huang et al., 2017) and used for the ONI calculation. Average SST for the Niño 3.4 region was calculated for each month, and further averaged using values from previous and following months. This three-month average was compared with the 30-year average and the difference was the ONI value for

the three-month considered. NOAA uses ONI as the primary index for identifying El Niño (warm) and La Niña (cool) events in the tropical Pacific. When the index is 0.5°C or higher, El Niño conditions exist and when the index is −0.5°C or lower, La Niña conditions exist.

Three ENSO indices namely, Southern Oscillation Index (SOI), Multivariate ENSO Index (MEI) and NINO3.4 have been correlated with WS in the present study. Monthly data for the above three indices were accessed from http://www.esrl.noaa.gov/psd/data/climateindices/. The SOI index is the difference between the atmospheric pressure at sea level at Tahiti and Darwin. Prolonged periods of negative (positive) SOI values coincide with El Niño (La Niña) episodes. SST anomalies equal to or greater than ±0.5°C in the Niño 3 region (5°N—5°S,150°W—90°W) are indicative of ENSO warm (cold) phase conditions. The Multivariate ENSO Index (MEI) is based on the six main observed variables over the tropical Pacific. These six variables are sea-level pressure, zonal and meridional components of the surface wind, sea surface temperature, surface air temperature, and total cloudiness fraction of the sky. The MEI integrates more information than SST based indices and thus is more comprehensive.

Spatial correlation plots were generated depicting regions statistically significant for WS, SST and ENSO indices. To identify the significant correlation ranges probability or p-values were calculated at the 0.05 significance level. If the p-value is less than 0.05 then the Pearson correlation coefficient is considered statistically significant (Fisher, 1992).

The NAO index is based on the surface sea-level pressure difference between the subtropical high and the subpolar low. The polar pressure is taken near Iceland and the subtropical pressure is taken near the Azores. The first mode of rotated EOF analysis of monthly mean 500 millibar height anomaly data from 1950 to 2000 over 0—90°N latitude is considered as the NAO pattern (Barnston and Livezey, 1987). The AMO is a 65—80-year cycle of North Atlantic sea surface temperatures for 1856—1999 (Kerr, 2000). AMO warm phases occurred during 1860—1880 and 1940—1960, and cool phases during 1905—1925 and 1970—1990 (Enfield et al., 2001). The NAO index for January and AMO index for July for the period 1950—2016 have been compared with the PC1 of WS.

In the first experiment, spatial correlation plots were generated between WS and SST data for all the 67 years to analyze the local impact. To explore how WS is influenced by remote ENSO indices (SOI, MEI, NINO3.4) respective spatial correlation plots were generated. Instead of all the 67 years together next particular years representing normal, El Niño and La Niña phases were taken into account for analysis. The above experiments were repeated and correlation plots generated for the particular phases.

Empirical orthogonal function (EOF) analysis is a powerful tool for data compression and dimensionality reduction. The EOF technique decomposes the space-time distributed data into spatial modes ranked by their temporal variances. Since EOFs have been introduced in atmospheric science by Lorenz (1956), it has become a statistical tool of fundamental importance in the atmosphere, ocean, and climate science for exploratory data analysis and dynamical mode reduction. Spectral analysis is a tool for extracting embedded structures in a time series. In particular, Fourier analysis has been used extensively by researchers for extracting deterministic structures from time series but is incapable of detecting non-stationary features often present in geophysical time series. Wavelet analysis can extract transient features embedded in time series, with a wavelet power spectrum representing variance (power) of a time series as a function of time and period. Since the work of Torrence and Compo (1998), wavelet analysis has been applied extensively to geophysical time series such as the indices for the North Atlantic Oscillation (Olsen et al., 2012) and Arctic Oscillation (Jevrejeva et al., 2003). The application of wavelet coherence and cross-wavelet analyses (Grinsted et al., 2004), moreover, has proven useful in relating geophysical time series to other time series (Jevrejeva et al., 2003).

Considering July and January representing the southwest and northeast monsoon periods, EOF analysis is applied on WS data for the BOB region (78°E to 98°E and 25°N to 5°N) for the analyzed period. The time series of the first principal components were linked to the NAO and AMO to establish a relationship between the WS variability and the ENSO indices. The localized intermittent periodicities can be identified on the time series data using continuous wavelet transforms, that expands a time series into a time-frequency space. The periodicity of the first principal components (PC1) of WS data was assessed using the wavelet method. Continuous wavelet power spectra were generated for analysis. Finally, wavelet coherence was applied to PC1 of WS and the ENSO indices to examine possible relationships between them. Coherence plots were generated between the two time series in both the time and frequency domain.

3. Results and discussions

3.1. Relationship between WS data, SST data and ENSO indices for IO

WS data were explored for the Indian Ocean region (30°E—120°E and 30°N—70°S) for July and January representing the southwest and northeast monsoons respectively. Spatial correlation plots were generated at a 95% confidence interval to analyze how WS, SST, and ENSO indices were related. To test if the correlation values are statistically significant, p-values were calculated (Table 1) at 0.05 significance level. Figure 1a and b depict significantly correlated regions for January and July representing opposite monsoon phases between WS and SST for all the 67 years. Considering the northern Indian Ocean, there was a negative correlation between WS and SST over BOB during July. It indicated higher (lower) WS at lower (higher) SST values. Figures 2—4 show how WS and SST correlated differently in the study area during the normal, El Niño and La Niña years for the above mentioned period. During the normal years (July) there was a significant negative correlation over BOB which fades away from La Niña to El Niño years. During the El Niño years, there was a significant negative correlation between WS and SST off the west coast of India in January and a positive correlation off the coast of Sri Lanka during July. During the La Niña years, there was a significant negative correlation over parts of BOB during July and a significant positive correlation off the Somali coast during January. Thus during El Niño events, the influence of local SST on the WS value decreased in the northern Indian Ocean in July whereas it increased on the

Table 1 p-values calculated to test if the correlation (r) is significant at 0.05 significance level for the period 1950–2016 (N=67). First all the January (JAN) months and all the July (JUL) months were considered. Then the above period was classified as normal or El Niño or La Niña year and tested.

(r)	All JAN 1950–2016 N=67 p-value	All JUL 1950–2016 N=67 p-value	Normal JAN N=22 p-value	Normal JUL N=33 p-value	El Niño JAN N=25 p-value	El Niño JUL N=17 p-value	La Niña JAN N=20 p-value	La Niña JUL N=17 p-value
1	0.00001	0.00001	0.00001	0.00001	0.00001	0.00001	0.00001	0.00001
0.8	0.00001	0.00001	0.00001	0.00001	0.00001	0.0001	0.00001	0.0001
0.6	0.00001	0.00001	0.0031	0.0002	0.0015	0.0109	0.0052	0.0109
0.5	0.00001	0.00001	0.0178	0.0030	0.0109	0.0409	0.0248	0.0409
0.45	0.00013	0.00013	0.0356	0.0086	0.0240	0.0699	0.0465	0.0699
0.4	0.0008	0.0008	0.0651	0.0211	0.0476	0.1116	0.0805	0.1116
0.35	0.0037	0.0037	0.1103	0.0458	0.0863	0.1684	0.1303	0.1684
0.3	0.0136	0.0136	0.1749	0.0898	0.1451	0.2420	0.1988	0.2420
0.25	0.0413	0.0413	0.2618	0.1606	0.2281	0.3331	0.2878	0.3331
0.2	0.1046	0.1046	0.3722	0.2644	0.3378	0.4415	0.3979	0.4415
0	1	1	1	1	1	1	1	1
−0.2	0.1046	0.1046	0.3722	0.2644	0.3378	0.4415	0.3979	0.4415
−0.25	0.0413	0.0413	0.2618	0.1606	0.2281	0.3331	0.2878	0.3331
−0.3	0.0136	0.0136	0.1749	0.0898	0.1451	0.2420	0.1988	0.2420
−0.35	0.0037	0.0037	0.1103	0.0458	0.0863	0.1684	0.1303	0.1684
−0.4	0.0008	0.0008	0.0651	0.0211	0.0476	0.1116	0.0805	0.1116
−0.45	0.00013	0.00013	0.0356	0.0086	0.0240	0.0699	0.0465	0.0699
−0.5	0.00001	0.00001	0.0178	0.0030	0.0109	0.0409	0.0248	0.0409
−0.6	0.00001	0.00001	0.0031	0.0002	0.0015	0.0109	0.0052	0.0109
−0.8	0.00001	0.00001	0.00001	0.00001	0.00001	0.0001	0.00001	0.0001
−1	0.00001	0.00001	0.00001	0.00001	0.00001	0.00001	0.00001	0.00001

(If the p-value is less than the significance level $\alpha = 0.05$ then r is significant).

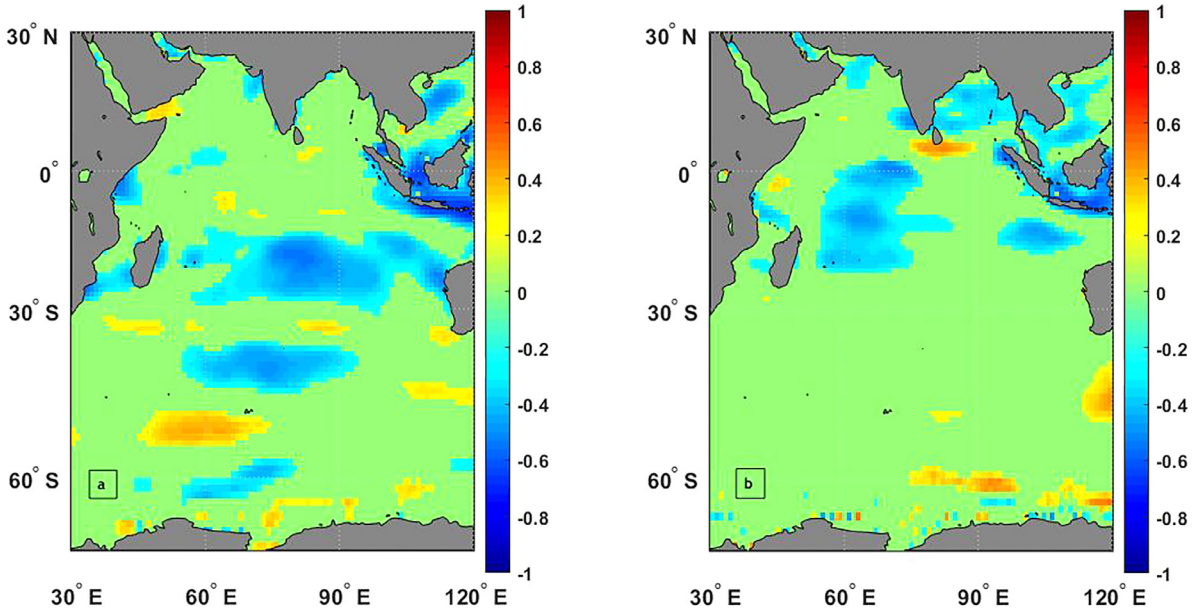

Figure 1 Significantly correlated regions between WS and SST at 95% confidence interval for (a) all January months (1950–2016) and (b) all July months (1950–2016).

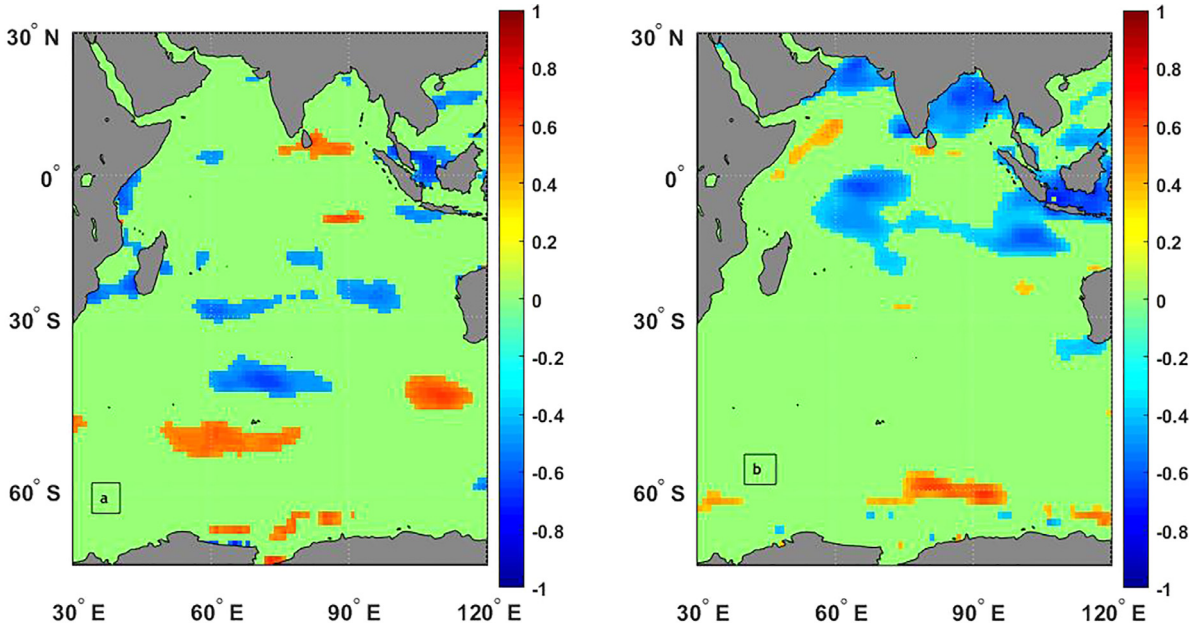

Figure 2 Significantly correlated regions between WS and SST at 95% confidence interval for (a) normal January months (22 years) and (b) normal July months (33 years).

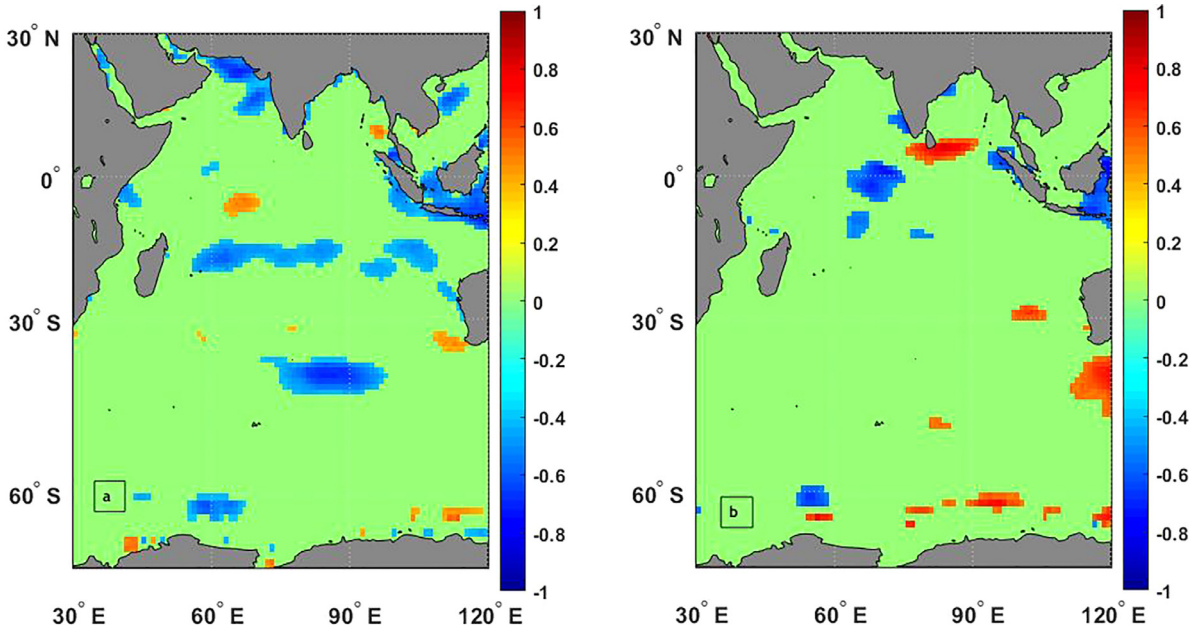

Figure 3 Significantly correlated regions between WS and SST at 95% confidence interval for (a) El Niño January months (25 years) and (b) El Niño July months (17 years).

west coast of India in January. Between 30°S and 60°S, there were both positively and negatively significantly correlated regions in January considering the normal years. These patches of correlated regions again faded away from La Niña to El Niño years. In July the Southern Indian Ocean was however uncorrelated in terms of WS and SST parameters.

The six plots in Fig. 5 depicts significant correlation regions between WS and the ENSO indices namely SOI, MEI and NINO3.4 for the normal January and July months respectively. During January there was a negative correlation between WS and SOI off Sri Lanka and southern part of the west coast of India and positive correlation with MEI and NINO3.4 for the same regions. As per the definitions of the indices opposite correlation signs were justified. The correlation patterns indicated the teleconnection features of the wind parameters with the ENSO indices. Figure 6 gave similar six plots for El Niño years and subsequently Fig. 7 for La Niña years. During the January El Niño episodes, the WS was significantly positively correlated with the MEI and NINO3.4 indices over a large area off Sri Lanka. In July the

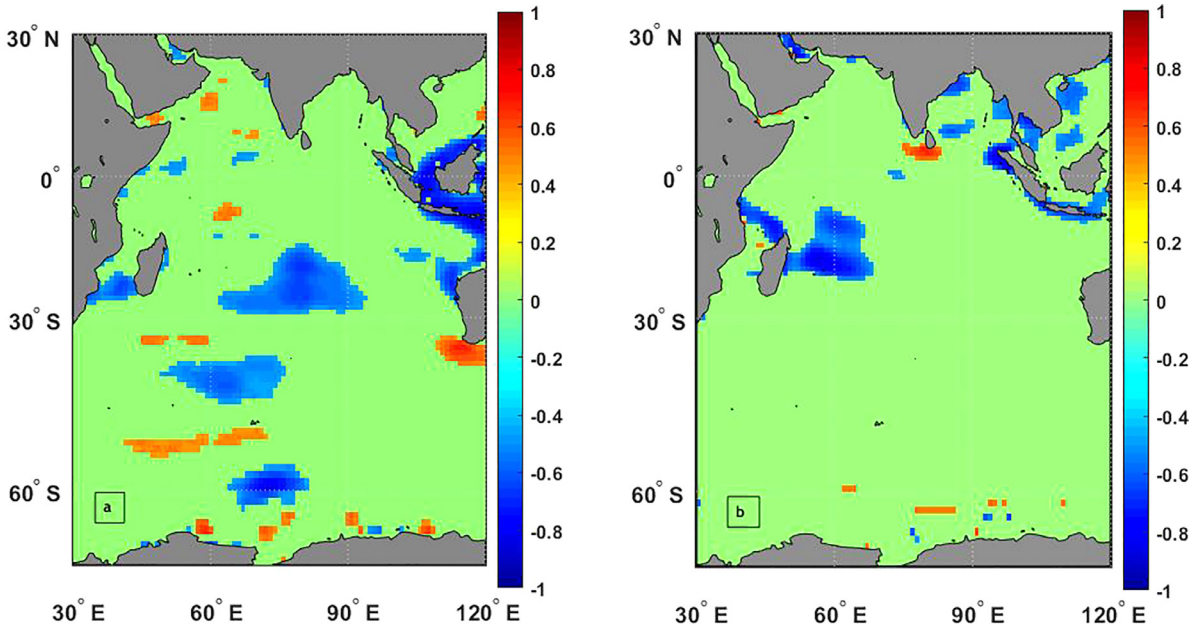

Figure 4 Significantly correlated regions between WS and SST at 95% confidence interval for (a) La Niña January months (20 years) and (b) La Niña July months (17 years).

influence was over a smaller area. However, such an impact was absent during the La Niña years.

3.2. EOF analysis and wavelet analysis for WS data of BOB region

EOF analysis was applied to the WS data of the BOB region (25°N to 5°N and 77.5°E to 100°E) for the analyzed period to extract the dominant mode representing the maximum variability. For January the first eigenmode accounted for 42.9% of the total variability of the WS data for the BOB region. Figure 8c depicts the spatial pattern of the first eigenmode of WS data. The maximum loading at the central BOB may be attributed to the northeast monsoon winds. The other eigenvectors contributed insignificantly and thus were not discussed. The PC1 corresponding to the first eigenmode is given in Fig. 8a, in which the maximum value occurred in 2007, while a deep fluctuation giving a minimum value in 2008. The high (low) peaks in the temporal pattern exhibited by the WS-PC1 corresponds to the negative (positive) NAO events (Fig. 8e). Thus, in general, an inverse relationship (negative correlation) between the NAO and the WS in the BOB region during the winter monsoon was observed, although there were few instances of positive correlation in the late 1960s and the mid-1980s. For July the first eigenmode accounted for 49.1% of the total variability of the WS data and Fig. 8d depicts maximum loading at the head Bay. The corresponding PC1 is given in Fig. 8b. The temporal pattern gave a maximum in 1962, a minimum in 1964. Again an inverse relationship can be established between the July WS-PC1 and the AMO which have a decreasing trend during 1962 and an increasing trend during 1965 (Fig. 8f). Standardized time series were considered in Fig. 8e and f for effective comparison.

The PC1 of WS data corresponding to January and July were normalized by their standard deviation and then were decomposed using the Morlet wavelet function. The Morlet wavelets are non-orthogonal wavelet functions that are useful for time series analysis. The continuous wavelet power spectra were generated with the cone of influence, where edge effects become important. Anything outside it limits the ability to interpret the results. The black contour enclosed regions of greater than 95% confidence for a red-noise process with a lag-1 coefficient of 0.52 (January) and 0.21 (July). The continuous wavelet power spectra generated exhibits significant regions in the 2—4-year band which corresponds to the ENSO oscillations having 2—7-year periodicity. In Fig. 9a representing the power spectrum in January the maximum power occurred during 2007 in the 2—4-year period. This matches the maximum value during 2007 in Fig. 8a representing the PC1 of WS data. Similarly, for July, the maximum power in Fig. 9b matches with the maximum value in Fig. 8b corresponding to the period 1962—64. Thus for the 67 years BOB WS data, the red-noise wavelet power spectra exhibits 2—4-year period oscillations which maybe teleconnected with the ENSO variability occurring in the 2—7-year band.

Wavelet coherence is a measure of the correlation between two time-series in the time-frequency plane. The relative phase relationship between the two time-series is shown with arrows. This can also be interpreted as a lead or a lag. Phase arrows pointing right or left represents an in-phase or anti-phase relationship. For two time-series X and Y phase arrows pointing down say X leading Y by 90 degrees. A lead of 90 degrees can also be interpreted as a lag of 270 degrees or a lag of 90 degrees relative to the anti-phase (opposite sign). Figure 10a and b displays the wavelet coherence between PC1-WS data and SOI index for January and July respectively for the analyzed period. In January and July, WS and SOI were in anti-phase (when one is maximum, the other is minimum and vice versa) in the 32-year period but were very insignificantly. From Fig. 10a,

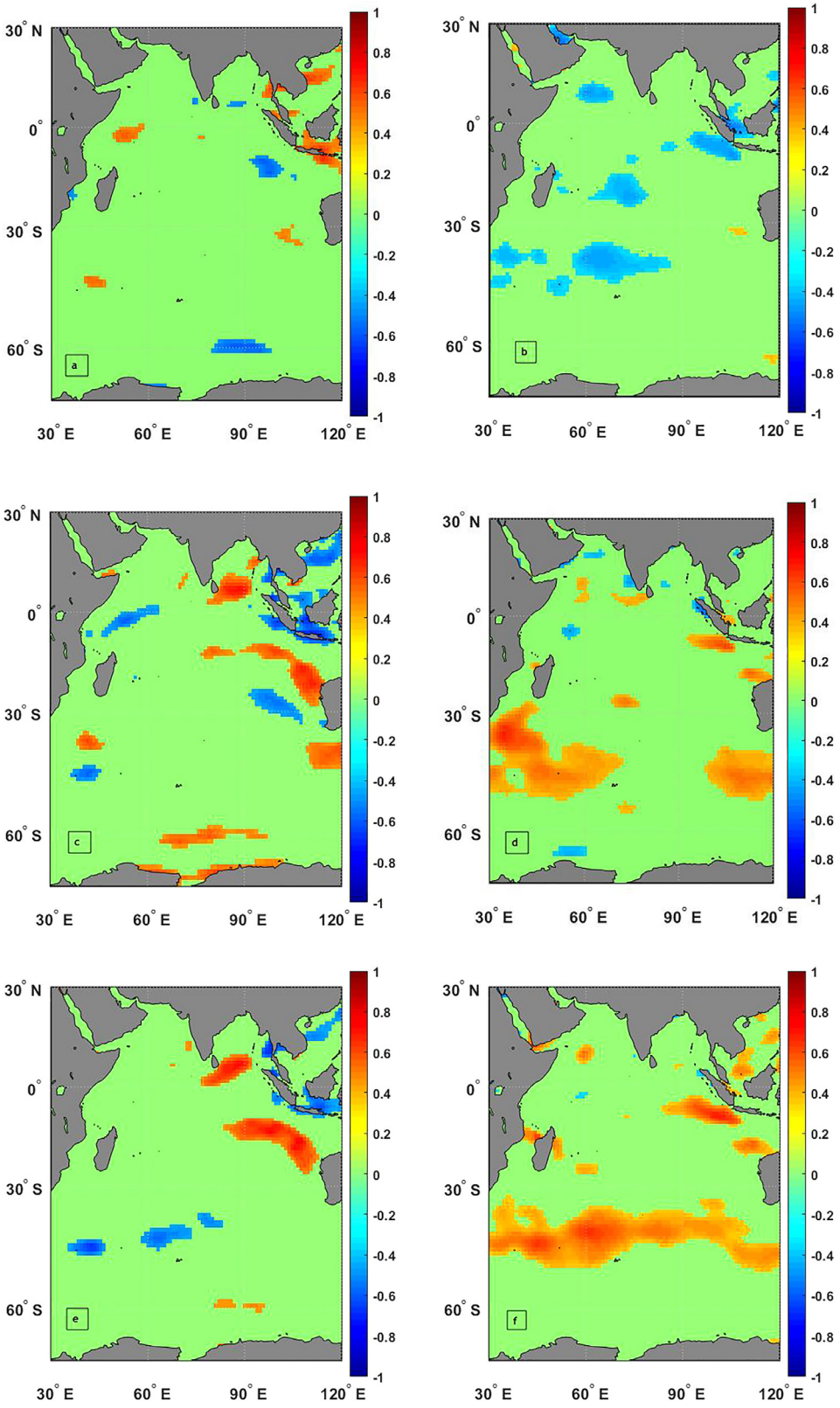

Figure 5 Significantly correlated regions at 95% confidence interval (a) between WS and SOI for 22 normal January months and (b) between WS and SOI for 33 normal July months and (c) between WS and MEI for 22 normal January months and (d) between WS and MEI for 33 normal July months and (e) between WS and NINO3.4 for 22 normal January months and (f) between WS and NINO3.4 for 33 normal July months.

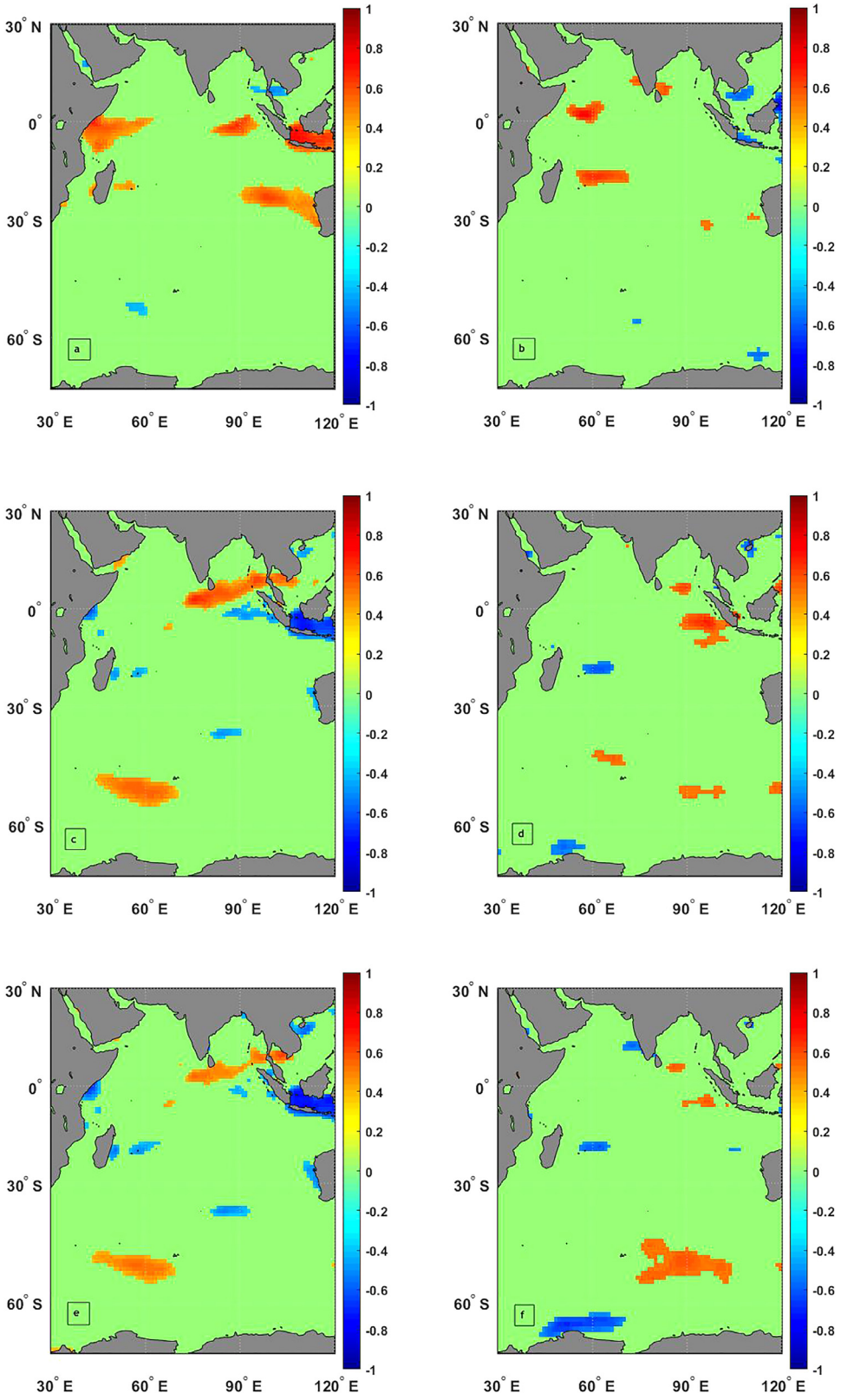

Figure 6 Significantly correlated regions at 95% confidence interval (a) between WS and SOI for 25 El Niño January months and (b) between WS and SOI for 17 El Niño July months and (c) between WS and MEI for 25 El Niño January months and (d) between WS and MEI for 17 El Niño July months and (e) between WS and NINO3.4 for 25 El Niño January months and (f) between WS and NINO3.4 for 17 El Niño July months.

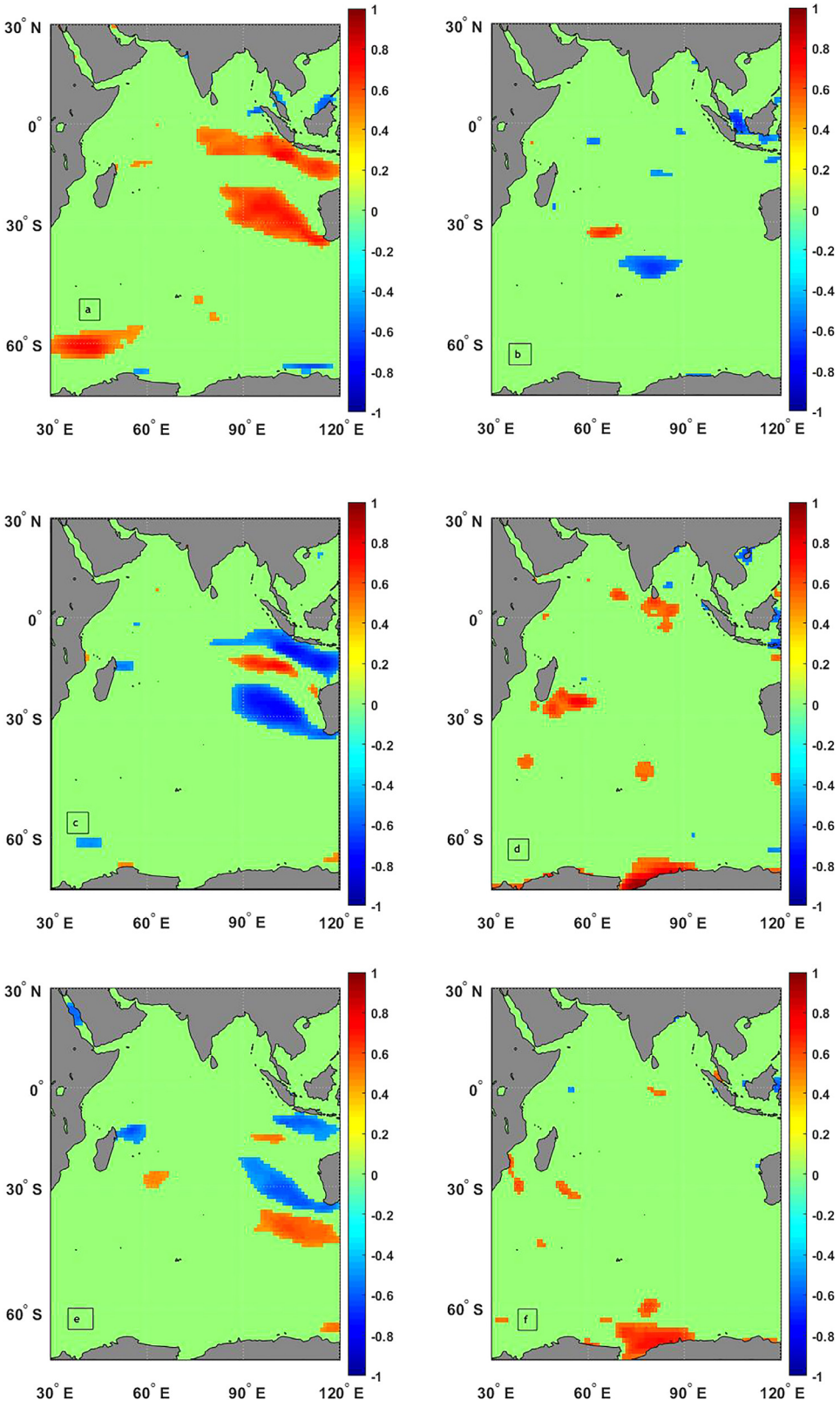

Figure 7 Significantly correlated regions at 95% confidence interval (a) between WS and SOI for 20 La Niña January months and (b) between WS and SOI for 17 La Niña July months and (c) between WS and MEI for 20 La Niña January months and (d) between WS and MEI for 17 La Niña July months and (e) between WS and NINO3.4 for 20 La Niña January months and (f) between WS and NINO3.4 for 17 La Niña July months.

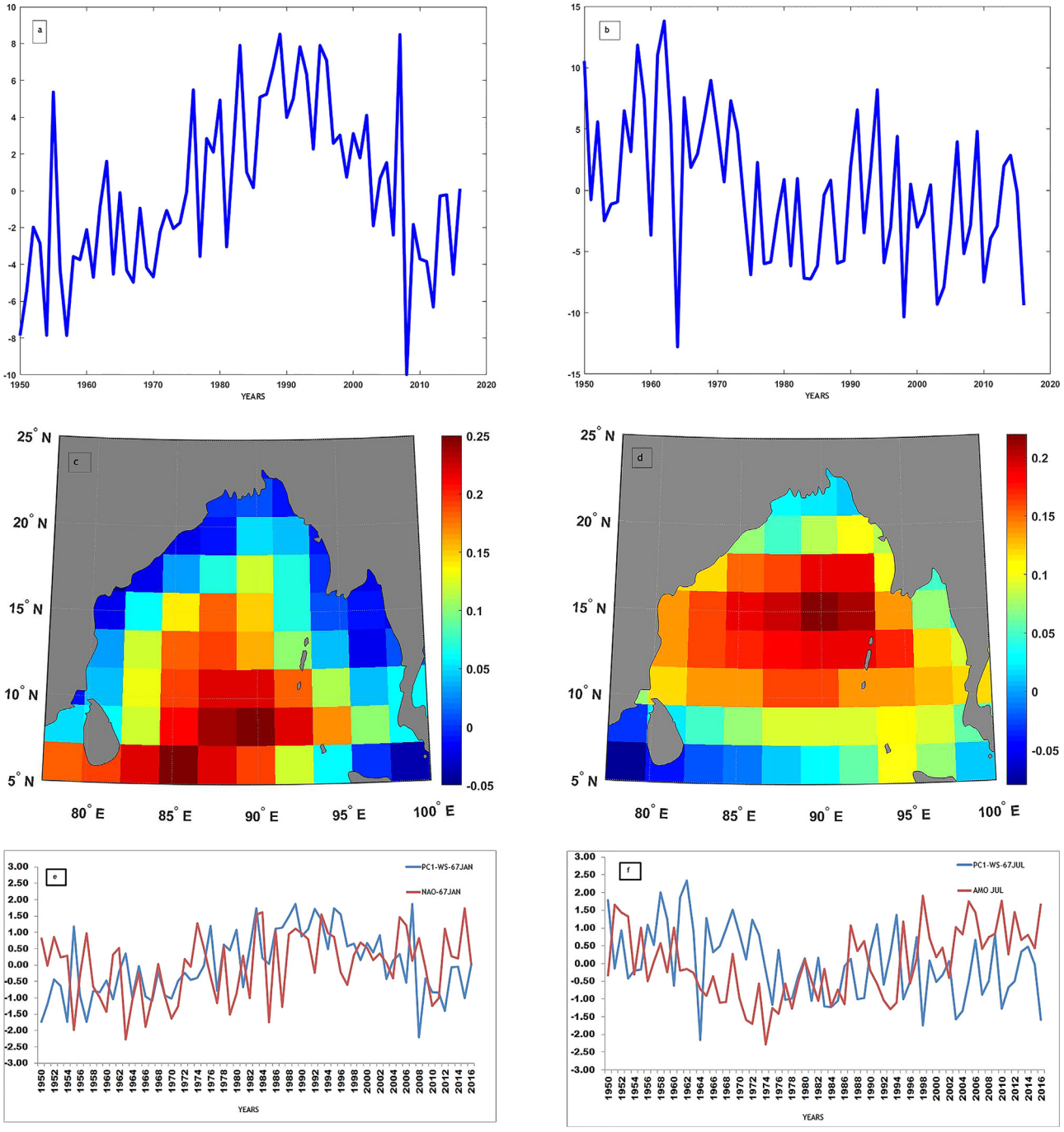

Figure 8 For the BOB WS data (1950—2016) (a) the PC1 for January and (b) the PC1 for July and (c) the first spatial eigenmode (42.9%) for January and (d) the first spatial eigenmode (49.1%) for July and (e) comparison between standardized WS-PC1 and NAO for January and (f) comparison between standardized WS-PC1 and AMO for July.

it can be said, the coherency was greater than 0.8 during 1955—65 (from x-axis) in the 8—16-year band (from y-axis). Figure 10b shows higher coherency regions in the 0—4-year period with both in-phase and anti-phase relationships. Figure 11a and b gave the wavelet coherence between PC1-WS data and MEI index for January and July respectively for the analyzed period with similar periodicities. In Fig. 11a there were again higher coherency regions in the 8—16-year period but with both in-phase and anti-phase relationships. Fig. 11b shows the in-phase relationship in the 0—4-year period along with higher coherency. Figure 12a and b gave similar plots with the NINO3.4 index. In January (Fig. 12a) and July (Fig. 12b) there were regions with higher coherency in the 8—16-year band and 0—4-year period respectively. An 8-year quasi-cyclic behavior of NAO may be the cause of the 8—16-year band coherency of WS variability with the ENSO indices. In July there was an in-phase relationship between WS and the ENSO indices in the 0—4-year band. This may

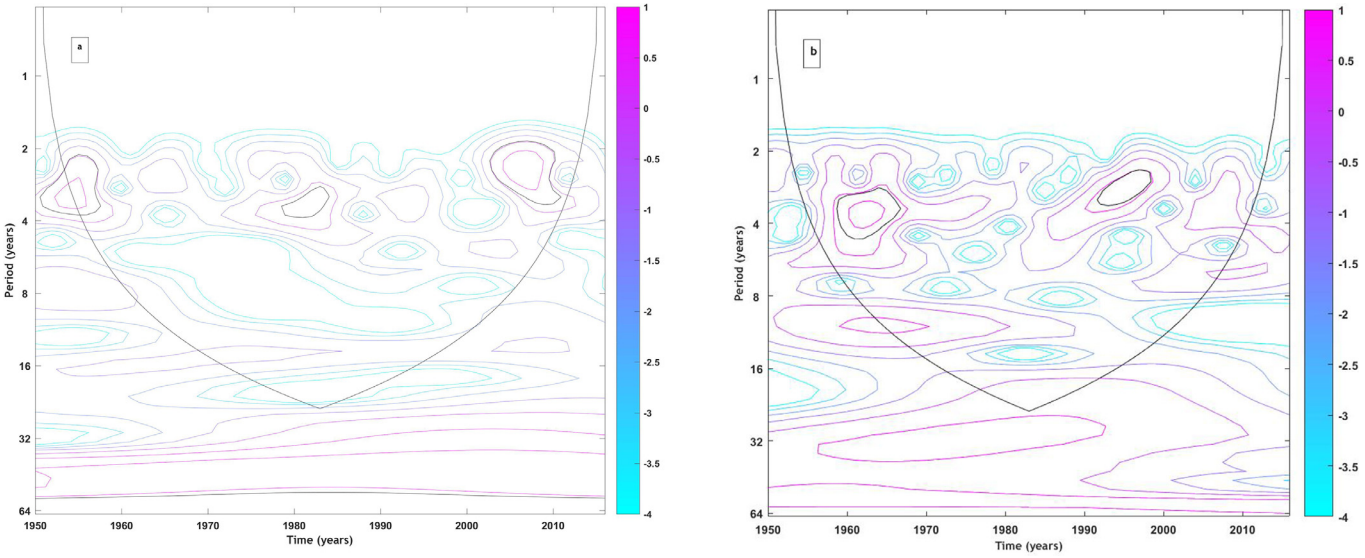

Figure 9 The continuous wavelet power spectrum of WS-PC1 along with the black contours which encircle the 5% significance regions, using a red-noise background spectrum, for (a) January and (b) July.

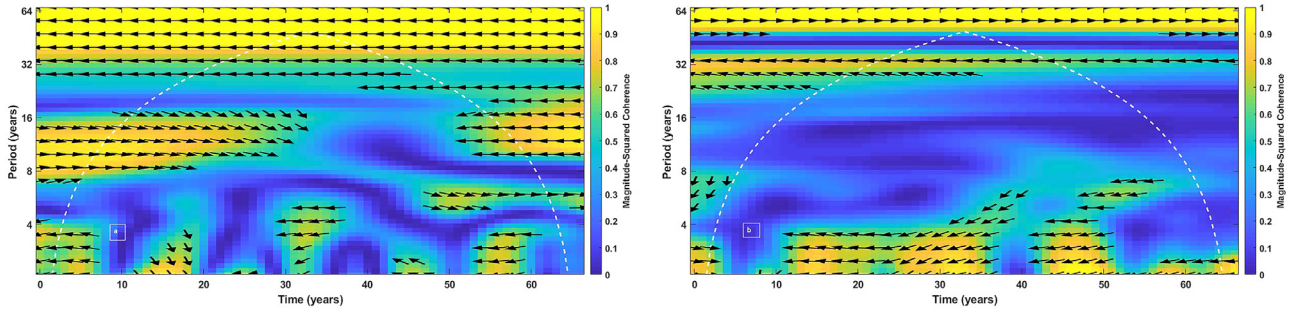

Figure 10 Squared wavelet coherence between PC1-WS and SOI time series for (a) January and (b) July.

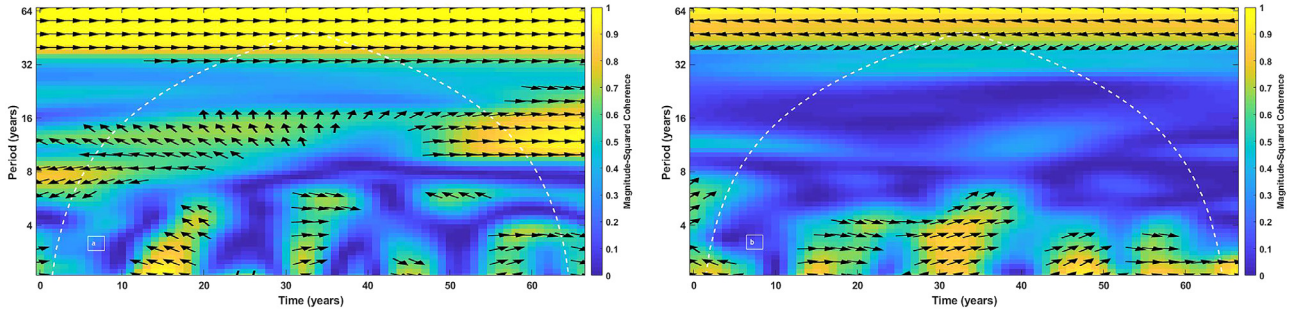

Figure 11 Squared wavelet coherence between PC1-WS and MEI time series for (a) January and (b) July.

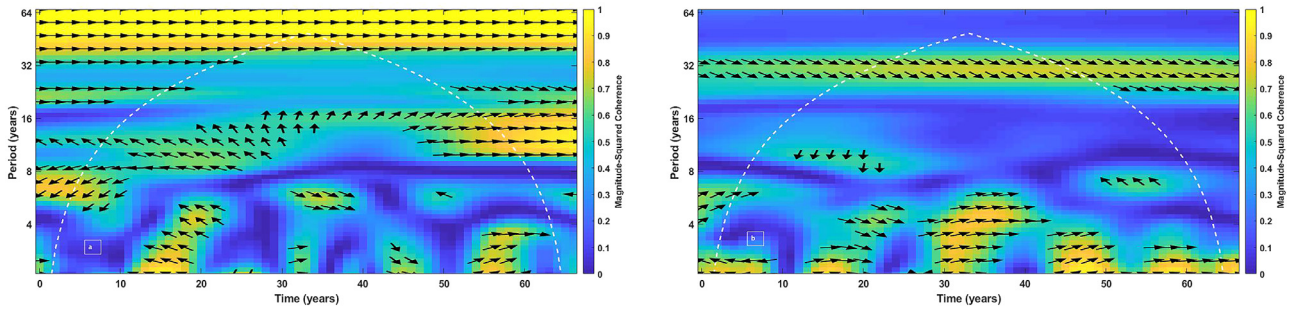

Figure 12 Squared wavelet coherence between PC1-WS and NINO3.4 time series for (a) January and (b) July.

be linked to the warm phases of AMO which are known to strengthen the summer monsoon rainfall over India.

4. Conclusions

An attempt has been made in the present work to explore how WS of the Indian Ocean region were influenced by the local SST and remote ENSO indices. Spatial correlation plots with significance level were generated between WS, SST data and the ENSO indices for July and January representing the southwest and northeast monsoons respectively. During the normal July months, there was a significant negative correlation between WS and SST over BOB which fades during El Niño years. Thus the SW monsoon locally impacted the WS and SST relationship. Next correlation plots were generated at a 95% confidence interval between WS and ENSO indices. Considering the normal January months WS had a significant negative correlation with SOI off the coast of Sri Lanka and south-west coast of India while the significant positive correlation with MEI and NINO3.4 for the same regions. During the El Niño years, WS had a significant positive correlation with MEI and NINO3.4 both, in January and July. Thus during the El Niño episodes, WS data was remotely influenced by the ENSO indices. During the La Niña years, there were no significant correlation patterns.

Further EOF analysis was applied to the WS data of the BOB region. For January the first eigenmode accounted for 42.9% and July 49.1% of the total variability. The January and July wind speed PCs were linked with the NAO and AMO oscillations respectively. The continuous wavelet power spectra of PC1 of WS data were generated for January and July. For both the red-noise wavelet power spectra, the significant regions occurred in the 2—4-year period replicating ENSO like oscillations. In January there were higher coherency values in the 8—16-year band which was related to the 8-year quasi-cyclic behavior of NAO. In July the higher coherency regions in the 0—4 year period were associated with the warm phases of the AMO which were known to strengthen the Indian summer monsoon rainfall. Thus patterns of global climate oscillations were compared to establish a close relationship between the WS variability and the ENSO indices in the BOB region.

Acknowledgments

This study is a part of a project no SR/FTP/ES80/2013 under Science and Engineering Research Board (SERB). It was sponsored by the Department of Science and Technology (DST), Government of India. The authors are grateful to DST for sponsoring the project.

References

Annamalai, H., Xie, S.P., McCreary, J.P., Murtugudde, R., 2005. Impact of Indian Ocean sea surface temperature on developing El Niño. J. Clim. 18, 302—319, http://dx.doi.org/10.1175/JCLI-3268.1.

Azad, S., Rajeevan, M., 2016. Possible shift in the ENSO-Indian monsoon rainfall relationship under future global warming. Nature Sci. Rep. 6 (1), art. no. 20145, 6 pp., http://dx.doi.org/10.1038/srep20145.

Barnston, A.G., Livezey, R.E., 1987. Classification, seasonality and persistence of low-frequency atmospheric circulation patterns. Mon. Weather Rev. 115, 1083—1126, http://dx.doi.org/10.1175/1520-0493(1987)115⟨1083:CSAPOL⟩2.0.CO;2.

Chen, W., Dong, B., Lu, R., 2010. Impact of the Atlantic Ocean on the multidecadal fluctuation of El Niño-Southern Oscillation-South Asian monsoon relationship in a Coupled General Circulation Model. J. Geophys. Res. 115 (D17), art. no. D17109, 12 pp., http://dx.doi.org/10.1029/2009JD013596.

Dong, L., McPhaden, M.J., 2018. Unusually warm Indian Ocean sea surface temperatures help to arrest development of El Niño in 2014. Nature Sci. Rep. 8, art. no. 2249, 10 pp., http://dx.doi.org/10.1038/s41598-018-20294-4.

Enfield, D.B., Mestas-Nunez, A.M., Trimble, P.J., 2001. The Atlantic Multidecadal Oscillation and its relationship to rainfall and river flows in the continental U.S. Geophys. Res. Lett. 28, 2077—2080, http://dx.doi.org/10.1029/2000GL012745.

Fan, F., Dong, X., Fang, X., Xue, F., Zheng, F., Zhu, J., 2017. Revisiting the relationship between the south Asian summer monsoon drought and El Niño warming pattern. Atmos. Sci. Lett. 18 (4), 175—182, http://dx.doi.org/10.1002/asl.740.

Fisher, R.A., 1992. Statistical Methods for Research Workers. In: Kotz, S., Johnson, N.L. (Eds.), Breakthroughs in Statistics. Springer Series in Statistics (Perspectives in Statistics). Springer, New York, 66—70, http://dx.doi.org/10.1007/978-1-4612-4380-9_6.

Goswami, B.N., Madhusoodanan, M.S., Neema, C.P., Sengupta, D., 2006. A physical mechanism for North Atlantic SST influence on the Indian summer monsoon. Geophys. Res. Lett. 33 (2), art. no. L02706, 4 pp., http://dx.doi.org/10.1029/2005GL024803.

Grinsted, A., Moore, J.C., Jevrejeva, S., 2004. Application of the CrossWavelet Transform and Wavelet Coherence to Geophysical Time Series. Nonlinear Proc. Geoph. 11, 561—566, http://dx.doi.org/10.5194/npg-11-561-2004.

Huang, C., Qiao, F., 2009. The relationship between sea surface temperature anomaly and wind energy input in the Pacific Ocean. Progr. Nat. Sci. 19 (10), 1409—1412, http://dx.doi.org/10.1016/j.pnsc.2009.03.004.

Huang, B., Thorne, P.W., Banzon, V.F., Boyer, T., Chepurin, G., Lawrimore, J.H., Menne, M.J., Smith, T.M., Vose, R.S., Zhang, H., 2017. Extended Reconstructed Sea Surface Temperature, Version 5 (ERSSTv5): Upgrades, Validations and Intercomparisons. J. Clim. 30, 8179—8205, http://dx.doi.org/10.1175/JCLI-D-16-0836.1.

Jevrejeva, S., Moore, J.C., Grinsted, A., 2003. Influence of the Arctic Oscillation and El Nino-Southern Oscillation (ENSO) on Ice Conditions in the Baltic Sea: The wavelet Approach. J. Geophys. Res. 108, art. no. D214677, 10 pp., http://dx.doi.org/10.1029/2003JD003417.

Kerr, R.A., 2000. A North Atlantic climate pacemaker for the centuries. Science 288 (5473), 1984—1986, http://dx.doi.org/10.1126/science.288.5473.1984.

Klein, S., Soden, A.B.J., Lau, N.C., 1999. Remote sea surface temperature variations during ENSO: Evidence for a tropical atmospheric bridge. J. Clim. 12, 917—932, http://dx.doi.org/10.1175/1520-0442(1999)012⟨0917:RSSTVD⟩2.0.CO;2.

Kug, J.S., Kang, I.S., 2006. Interactive feedback between ENSO and the Indian Ocean. J. Clim. 19, 1784—1801, http://dx.doi.org/10.1175/JCLI3660.1.

Kumar, K.K., Rajagopalan, B., Cane, M.A., 1999. On the weakening relationship between the Indian monsoon and ENSO. Science 284 (5423), 2156—2159, http://dx.doi.org/10.1126/science.284.5423.2156.

Li, T., Wang, B., Wu, B., Zhou, T., Chang, C.P., Zhang, R., 2017. Theories on formation of an anomalous anticyclone in western North Pacific during El Niño: A review. J. Meteorol. Res. 31 (6), 987—1006, http://dx.doi.org/10.1007/s13351-017-7147-6.

Li, T., Zhang, Y., Chang, C.P., Wang, B., 2001. On the relationship between Indian Ocean sea surface temperature and Asian summer monsoon. Geophys. Res. Lett. 28, 2843—2846, http://dx.doi.org/10.1029/2000GL011847.

Lorenz, E.N., 1956. Empirical orthogonal functions and statistical weather prediction. Statistical Forecast Project Report 1, Dept. of Meteor. MIT Tech. Rep. 49, 52 pp., https://eapsweb.mit.edu/sites/default/files/Empirical_Orthogonal_Functions_1956.pdf.

McPhaden, M.J., 2002. El Niño and La Niña: Causes and global consequences, in Encyclopedia of Global Environmental Change. John Wiley, Chichester, U.K, 353—370, https://www.pmel.noaa.gov/gtmba/files/PDF/pubs/ElNinoLaNina.pdf.

Okumura, M.Y., Deser, C., 2010. Asymmetry in the Duration of El Niño and La Niña. J. Clim. 23 (21), 5826—5843, http://dx.doi.org/10.1175/2010JCLI3592.1.

Olsen, J., Anderson, J.N., Knudsen, M.F., 2012. Variability of the North Atlantic Oscillation over the past 5200 years. Nat. Geosci. 5, 808—812, http://dx.doi.org/10.1038/ngeo1589.

Schott, F.A., Xie, S.P., McCreary Jr., J.P., 2009. Indian Ocean circulation and climate variability. Rev. Geophys. 47, art. no. RG1002, 46 pp., http://dx.doi.org/10.1029/2007RG000245.

Sun, B., Wang, H., 2019. Enhanced connections between summer precipitation over the Three-River-Source region of China and the global climate system. Climate Dynamics 52 (5—6), 3471—3488, http://dx.doi.org/10.1007/s00382-018-4326-9.

Torrence, C., Compo, G.P., 1998. A Practical Guide to Wavelet Analysis. Bull. Am. Meteorol. Soc. 79, 61—78, http://dx.doi.org/10.1175/1520-0477(1998)079⟨0061:APGTWA⟩2.0.CO;2.

Venzke, S., Latif, M., Villwock, A., 2000. The coupled GCM ECHO-2. Part II: Indian Ocean response to ENSO. J. Clim. 13, 1371—1383, http://dx.doi.org/10.1175/1520-0442(2000)013⟨1371:TCGE⟩2.0.CO;2.

Xie, S.P., Kosaka, Y., Du, Y., Hu, K., Chowdary, J.S., Huang, G., 2016. Indo-western Pacific ocean capacitor and coherent climate anomalies in post-ENSO summer: A review. Adv. Atmos. Sci. 33 (4), 411—432, http://dx.doi.org/10.1007/s00376-015-5192-6.